Folded optical design for high fidelity atmospheric emulation with a spatial light modulator

Sarah A. Tedder*, Yousef Chahine
NASA Glenn Research Center, 21000 Brookpark Rd, Cleveland, OH, USA 44135-3127

ABSTRACT

Atmospheric emulators based on spatial light modulators offer the ability to test atmospheric propagation effects on a laser communication component's performance in the laboratory setting. To create a high-fidelity atmospheric emulator, details of the optical design are key. This paper discusses the optical design choices and refinements that enabled the creation of a system that was verified to recreate multi-layer turbulence with high fidelity up to D/r_0 =50. Optical design choices that affect the fidelity discussed in this paper include the characteristics of the input laser, the spatial light modulator, the holograms, the image relay optical components, and the spatial filter. Also included in this paper is a comparison of the chosen folded optical layout to an alternative angled layout.

Keywords: Atmospheric turbulence, optical design, free-space laser communications.

1. INTRODUCTION

Atmospheric emulators made with spatial light modulators (SLMs) offer the ability to test a laser communication component's performance while in the laboratory with a broad range of turbulence levels[1-13]. When compared to rotating phase plates[14-18] (another common option for emulating atmosphere in the laboratory), SLM based systems have a speed limitation, restricting real time recreation of atmospheric optical turbulence evolving at typical Greenwood frequencies. This limitation is caused by the SLM's response time and varies depending on the SLM and wavelength. At visible wavelengths (λ) response time is fast enough for recreating expected Greenwood frequencies as in Refs. [2, 6, and 8]. The response time increases with wavelength so at optical communications C-band wavelengths a typical response time is 250 ms. This limitation means SLM-based systems have not been typically used for testing real time effects on communication systems in C-band but can be used in a static fashion to evaluate components and systems statistically[19].

Although rotating plates have the advantage in real-time emulation, they require a new phase plate to be designed and fabricated for each new turbulence condition (beam diameter to Fried parameter ratio, D/r_0). The SLM setup only requires a new set of images to be created via a computer, requiring less time and materials for testing a wide range of atmospheric conditions. Another advantage the SLM method offers is the ability to add other optical train effects such as apertures, obscurations, or curvatures, by just changing the computer-generated image. A system using phase plates would require a change or addition of optics to include these effects. Finally, unlike rotating phase plates, SLM-based emulators offer the possibility of playing back measured atmospheric effects from operational links.

Commonly, SLM-based emulators are designed using a phase screen approach [1,4,6, 9, 10]. The phase screen approach loses fidelity for lower elevation propagation paths due to the intensity nulls which form in conjunction with branch points in deep turbulence. The phase screen approach also requires one SLM for every atmospheric layer; therefore, to implement a full atmospheric propagation from space to ground, many SLMs may be needed. In contrast, using a

*sarah.a.tedder@nasa.gov; www.nasa.gov

holographic method allows emulation with as many layers as desired with one SLM. Holography also eliminates the need for a propagation length to develop the intensity effects, as the hologram creates the desired final output at the surface of the SLM. The output can then be relocated to a convenient location with a 4f system. A spatial filter used in the holographic system also eliminates diffractive errors from the edge of the SLM, which can degrade the fidelity of systems using multiple SLMs in series[13]. However, it should be noted that the holographic system does not emulate the same transfer operator as a system using multiple SLMs as phase screens, so multi-SLM systems still have certain benefits for emulating the propagation of non-plane wave free-space modes through turbulent channels (see Appendix A).

We presented a holographic SLM-based atmospheric emulator in Ref. [12]. In addition to emulating atmospheric turbulence, this system reforms the light into an arbitrary spatial mode and is hence referred to as the arbitrary light field generator (ALF-G). The optical layout of the ALF-G is reprinted from Ref. [12] in Figure 1. Ref. [12] focused on the verification of this system using a wavefront sensor to recreate multi-layer turbulence with high fidelity up to D/r_0 =50. The details of the optical design were key to creating the high-fidelity performance of the atmospheric emulator. This paper discusses the optical design choices of that system and recent improvements.

Discussion about the ALF-G design is broken into sections focused on each system function. The discussion starts in Section 2 with the main component, the SLM. The rest of the system is broken into sections describing the input light (Section 3), the image relay and spatial filtering (Section 4). Section 5 describes unwanted reflections and how to remove them. Finally, Section 6 compares the selected folded optics layout to an alternative optical layout. In summary, this paper offers recommendations on how to build a high-fidelity atmospheric emulator with a folded layout.

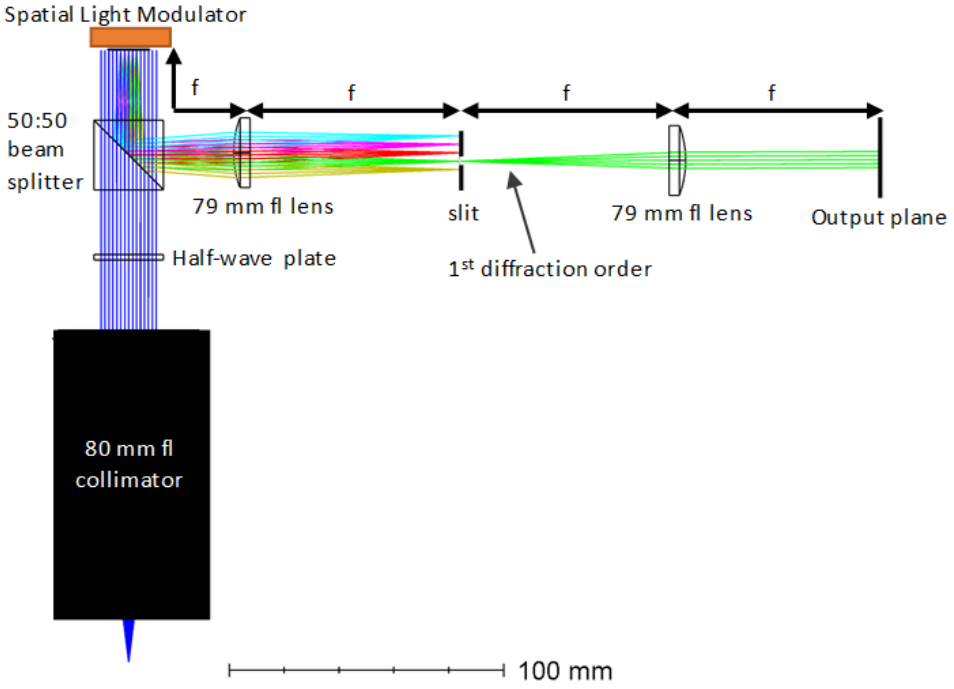

Figure 1. Optical layout of arbitrary light field generator (ALF-G). This diagram shows a ray trace of the ALF-G. The blue ray traces are the input light to the spatial light modulator. The yellow ray traces are the zero-order reflection from the SLM, green is the first-order reflection, red is the second-order reflection, purple is the third-order reflection, and cyan is the 4th-order reflection. The f represents 1 focal length of the lens.

2. SPATIAL LIGHT MODULATOR

The main component of the ALF-G is a reflective phase-only SLM, and the rest of the system is designed to support this component. Key features of the SLM that affect the performance of the system are the wavelength, number of

pixels, number of phase levels, and pixel response time. The ALF-G is designed to support optical communication applications at 1550 nm so the SLMs used in several versions of the system all supported C-band wavelengths.

The number of pixels available on the SLM determine the spatial resolution achievable in the emulation. But the final spatial resolution of the output beam is determined by the number of pixels used by the hologram to define the beam. For example, in Ref. 12 the SLM had a 15.36 × 9.6 mm surface area comprised of an array of 1920×1200 active liquid crystal elements with 8 μm pixel pitch. But after applying a hologram with a circular aperture with a diameter that is 70% diameter of the 1200 linear direction pixels (6.72 mm) only 840 addressable pixels were available.

Most C-band SLM have a pixel response time of a few hundred milliseconds, limiting the system refresh rate to a few Hz. For example, the SLM used in Ref. 12 had a response time of 250 ms, limiting the system to a ~2 Hz refresh rate and causing the system to be incapable of reproducing typical Greenwood frequencies.

The phase front resolution of the emulation output is determined by the number of distinct phase levels each pixel can impart. To achieve control of the intensity and phase with a phase only SLM, complex amplitude phase holograms can be used[20]. This method produces holograms with a limited phase range [-1.84,1.84]. Therefore, if an SLM is used for an ALF-G with 1024 phase levels from 0 to 2π, the complex amplitude phase hologram method reduces the number of usable phase levels to 600.

Complex amplitude phase holograms are created using vertical grating lines that create multiple output orders of modulated light at distinct angles relative to a zero-order, which is reflected at an angle equal to the angle of incidence (see Figure 1). The number of pixels in the grating period controls the size of the separation angle between diffraction orders and the range of spatial modes and the range of spatial modes obtainable in the output beam. In Ref. [12], it was found that 9 pixels per grating period produced optimum fidelity up to D/r_0=50, but depending on the application, less can be sufficient.

The reflective backplane of an SLM can a flat surface[12]; however, many SLM backplanes have significant curvature. In these cases, a calibration procedure can be employed to correct for the curvature with the holograms. For example, a wavefront sensor (WFS) with a well-calibrated absolute reference can be used to implement a simple compensation similar to that described in Ref. [4]. First, an image of the flat top beam is collected from the WFS placed at the output plane in Figure 1. The coefficients c_n^m for the first n radial orders of Zernike polynomials Z_n^m are calculated within the pupil. The associated phase profile $\phi_c = 2\pi \sum_{m,n} c_n^m Z_n^m$ is then subtracted from the phase ϕ of the desired beam before generating the hologram. It should be noted that this method can introduce aberrations from the WFS reference onto the beam. To prevent artificially introducing aberrations from the WFS reference, one can restrict the coefficients to remove only lower order aberrations (e.g. up to $n \leq 10$) depending on the accuracy of the WFS reference (more generally, depending on the absolute accuracy of the technique used to measure the Zernike coefficients). Nevertheless, calibration to remove residual aberrations may be unavoidable, particularly for those introduced by the SLM backplane.

The results from the application of this calibration procedure on an ALF-G built with an SLM with a curved backplane can be seen in Figure 2. Figure 2 shows images of the phase profile collected with a WFS before and after the compensation has been applied. In this case, the compensation improved the peak to valley wavefront error by 0.61λ and the root mean square error by 0.063λ, resulting in final values of .79λ and 0.037λ respectively.

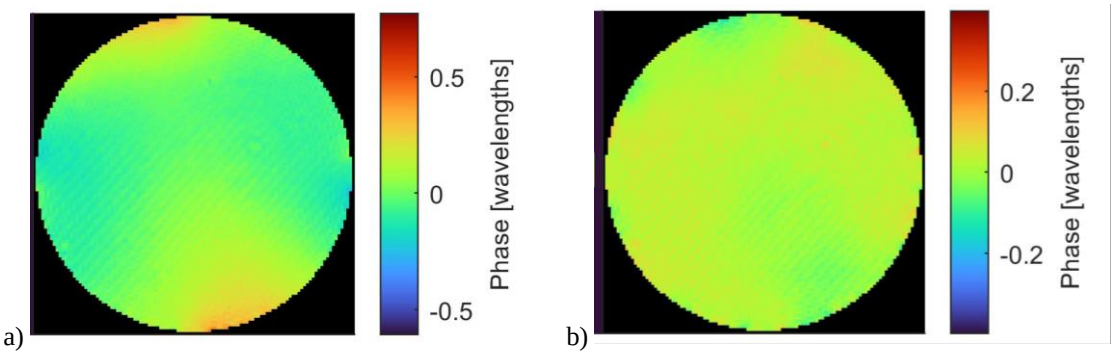

Figure 2. Images of the phase at the output plane of a flat-top beam created with an ALF-G and collected with a WFS. This ALF-G was built with an SLM with a curved backplane. Image a) was taken before compensation and image b) was taken after the compensation has been applied.

We recommend the SLM to be mounted independently to allow for rotation of the SLM surface relative to the rest of the optics. This enables the first-order of the modulated beam that is reflected from the SLM at an angle relative to the SLM surface to be aligned perpendicular to the rest of the optics. It also enables removal of reflections described below in Section 5. Otherwise, this alignment and removal of reflections will require translation of all the optics downstream of the SLM. The SLM mount needs to rotate around the SLM surface to avoid translating the reflected beam off-axis. If the provided mount for the SLM is not designed for this (most are not) a rotational and translational mount are needed to orient the SLM surface to pass only first-order modulated beam to the system output.

3. INPUT LIGHT

The ALF-G's input light source is a linearly polarized laser that was fiber coupled with polarization maintaining single-mode fiber. For the SLM to perform modulation, the input light is required to be linearly polarized because of the polarization-dependent phase modulation implemented by the SLM's liquid crystals. The polarization direction of the light was rotated using a half-wave plate (HWP) to the direction that maximized the power of the light modulated by the SLM.

Despite the modulation of the intensity and phase profile by the SLM, any remaining intensity variation in the input beam is carried over into the output beam. Therefore, the input light should be collimated to a size that fills the part of the SLM surface in use with a uniform intensity profile. To make the intensity close to uniform, we used an 80 mm focal length collimator to create a 14.5 mm diameter beam. This overfills the 6.72 mm diameter area that was in active use by the SLM as defined by the hologram. This produced a peak-to-valley wavefront error of ~.38λ and root mean square error of λ\40.[12]

4. IMAGE RELAYING AND SPATIAL FILTERING

A 4f system is employed to filter the diffraction orders and relay the field created by the hologram at the SLM plane to an output plane that is accessible. As seen in Figure 1, the 4f system starts at the SLM. The modulated light is turned by the 50:50 beam splitter (BS). In Ref. 12, a glass cube BS was used, but as discussed in Section 5, a pellicle offers another option to reduce unwanted reflections. The BS sends half of the remaining power into a focusing lens (L1). L1 is placed one focal length from the SLM. We chose a focal length of 79 mm for L1, but this can be adjusted for the desired system size or other spacing needs.

To filter the other diffraction orders created by the SLM an adjustable-width slit is placed at the focus of L1. The slit-width is set to $w = f\lambda/p$ depending on the hologram grating period, p, placing the blade edges exactly half-way between the diffraction orders. This blocks the other diffraction orders while allowing the maximum number of spatial frequencies to be transmitted through the system. The SLM surface is rotated and translated such that the first-order diffraction is centered with the slit while maintaining a centralized and perpendicular beam path relative to the optics. The light is then collimated with a second aspheric lens (L2) with matching focal length to L1. L2 is placed a focal length from the focal plane of L1. For the ease of alignment and stability, we recommend using cage mounts that connect the BS, L1, L2 and the slit.

Each of the diffraction orders have two copies created on each side of the zero-order, which differ by a conjugation of the phase. To ensure that the unconjugated first order reflection is chosen by the slit, a hologram generated to produce a focusing beam can be applied to the SLM. Then the beam is verified to focus past the output plane.

The desired output is located at the output plane in Figure 1. Examples of the input irradiance and phase at $D/r_0=20$ compared to the measured output, are shown in Figure 3.

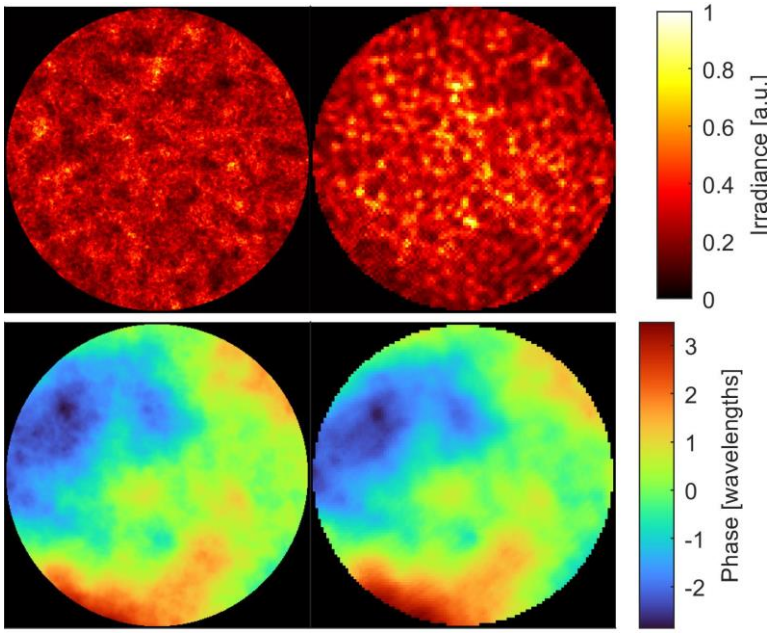

Figure 3. Input of the irradiance and phase compared to the measured output of a beam simulating optical turbulence with $D/r_0=20$. The left images are the input irradiance and phase. The right images are the measured irradiance and phase.

5. REFLECTIONS

When using the folded optical layout design in Figure 1, there are 3 reflections that can overlap with the signal at the image plane. This can cause errors in efficiency and wavefront measurements. All of these reflections can be eliminated with alignment changes. There are two sources of reflections: the internal surfaces of the glass cube BS and the curved surface of the collimator lens. We have imaged these reflections in Figure 4a by placing a camera with a 3 µm pixel resolution near at the focus of a 100 mm focal length lens. The lens was placed at the output plane (1 focal length downstream of L2). All 3 reflections and the signal were collected in the image shown in Figure 4a. Although Figure 4a shows the reflections spatially separated from the signal, if unchecked the alignment of the system can lead to an overlap. These reflections add to the noise and can have a significant amount of energy. For example, if all 3 reflections overlap with the signal for an emulation with $D/r_0=9$, the signal to reflection noise ratio is 1.76.

Two of the three reflections originate from the glass cube BS. These reflections have a focus at the same location as the signal. They are not modulated by the SLM. Unlike the signal, these reflections do not move when the SLM is rotated. Therefore, these reflections can be blocked by the slit by rotating and translating the SLM to move the signal away from them.

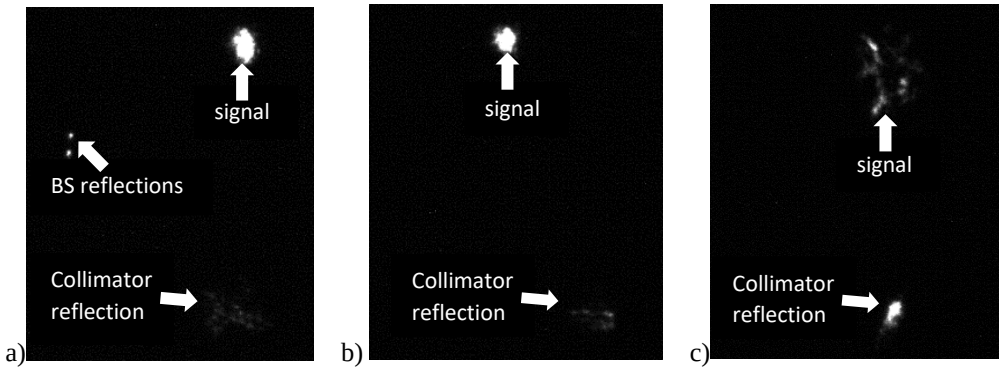

Figure 4. Images of ALF-G signal and unwanted reflections. Images in a) and b) are collected of the focus of a 100 mm lens placed at the image plane. a) is a system with a glass cube beam splitter and b) is a system with a pellicle beam splitter. c) is an image collected at the focus of the collimator reflection.

Another option that will eliminate the BS reflections is to replace the glass cube beam splitter with a pellicle. Figure 4(b) shows an image taken at the focus of a system using a pellicle. As shown in the image, only the signal and collimator surface reflection remain. Using the pellicle decreases the signal by 14% but increases the signal to reflection noise ratio to 4.06. This is because the pellicle not only eliminates the beam splitter reflections but reduces the energy from the collimator reflection by ~25%.

The third reflection is the zero-order modulation from SLM that passes back through the BS to the curved surface of the collimator. This has a focus in front of the signal as shown in the image collected in front of the 100 mm focus in Figure 4(c). This reflection does not move with alignment changes of the SLM surface but does move with the collimator realignment. Using a combination of translation of the collimator and rotation and translation for the SLM surface, the modulated signal can be moved away from this reflection. This allows the reflection to be blocked by the slit.

6. ALTERNATIVE OPTICAL LAYOUT

An alternative optical layout to the folded design presented in Fig. 1 is an angled layout shown in Figure 5. The angled layout has 1 less optic than the folded design eliminating the need for several passes of the light through a BS. This would increase the throughput of the angled layout over the folded layout by ~75%. Another advantage of the angled design is that it eliminates all reflections discussed above in Section 5. The angled layout has a narrower, longer footprint when compared to the folded design. The layout and build of the angled design adds the challenge of orienting and aligning optics to an acute angle. This is contrary to standard optical mechanical breadboards and mounts, however, it can be accomplished through specialized cage mounts[21]. Meadowlark accomplishes aligning to the acute angle with a specialized plate mounted to the SLM to hold cage mounts. For the SLM holographic setup this specialized plate would have to be mounted independently in angle and lateral adjustment to enable fine alignment of the first-order through the 4f system.

For our application, a lower throughput was not a concern, and we were able to eliminate the reflections achieving a high signal-to-noise ratio with alignment. Therefore, we selected the folded design to avoid the complication of mounting and aligning optics at an acute level and to achieve a squarer footprint.

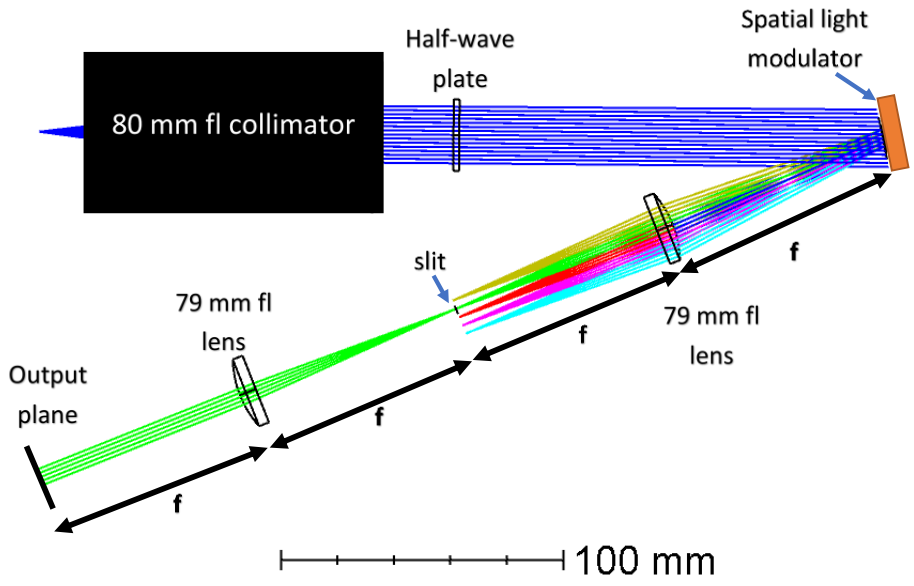

Figure 5. Angled optical layout of arbitrary light field generator (ALF-G). This diagram shows a ray trace of the ALF-G. The blue ray traces are the input light to the spatial light modulator. The yellow ray traces are the zero-order reflection from the SLM, green is the first-order reflection, red is the second-order reflection, purple is the third-order reflection, and cyan is the fourth-order reflection.

7. SUMMARY

In summary, we have presented recommendations for the folded optical design of a holographic SLM based system that can produce high fidelity atmospheric emulation. Our optical component specification recommendations include selecting an SLM with high spatial resolution, overfilling the SLM with a long focal length collimator lens, setting the filter at half the distance between the diffraction orders, and using a pellicle BS. Our optical mechanical recommendations include mounting the SLM on a rotational and translational mount and mounting the 4f system to the BS with a cage system. We also provided information on how procedures and calibrations can be performed to verify the conjugate diffraction order is selected, to remove SLM curvatures, and to remove unwanted reflections. We discussed the advantages an angled layout may offer and that we chose the folded layout for ease of alignment.

Our next step is the addition of continuous wave background light. This will enable us to use the ALF-G to perform code word error rate testing of a photon counting real-time receiver. Other future work will include the build and testing of a C-band ALF-G capable of real time emulation of Greenwood frequencies in the hundreds of hertz using SLM's newly on the market in the last few years[21,22]. These new systems may allow the SLM method to overcome its main drawback when compared to rotating phase plates. Complimentary future work will include using wave front sensor measurements of atmospheric data to turn this higher speed ALF-G into a playback system. Another future consideration is the use of a digital micromirror device as the SLM[23] instead of the liquid crystal device used here.

REFERENCES

[1] M. K. Giles, A. Seward, M. A. Vorontsov, J. Rha, and R. Jimenez, "Setting up a liquid crystal phase screen to simulate atmospheric turbulence," Proc. SPIE 4124, 89-97 (2000).

[2] T. S. Taylor and D. A. Gregory, "Laboratory simulation of atmospheric turbulence-induced optical wavefront distortion," Opt. Laser Technol. 34, 665-669 (2002)

[3] L. Hu, L. Xuan, Z. Cao, Q. Mu, D. Li, and Y. Liu, "A liquid crystal atmospheric turbulence simulator," Opt. Express 14, 11911-11918 (2006).

[4] Jason D. Schmidt, Matthew E. Goda, Bradley D. Duncan, "Aberration production using a high-resolution liquid-crystal spatial light modulator.", Applied optics 46(13), pg. 2423, (2007); doi:10.1364/ao.46.002423

[5] Christopher C. Wilcox, Ty Martinez, Freddie Santiago, Jonathan R. Andrews, Sergio R. Restaino, Scott W. Teare, and Don Payne "Atmospheric simulator for testing adaptive optic systems", Proc. SPIE 7015, Adaptive Optics Systems, 701542 (14 July 2008); https://doi.org/10.1117/12.789464

[6] Lifa Hu, Li Xuan, Dayu Li, Zhaoliang Cao, Quanquan Mu, Yonggang Liu, Zenghui Peng, and Xinhai Lu, "Real-time liquid-crystal atmosphere turbulence simulator with graphic processing unit," Opt. Express 17, 7259-7268 (2009)

[7] Italo Toselli, Brij N. Agrawal, Christopher C. Wilcox, and Sergio Restaino "Experimental generation of non-Kolmogorov turbulence using a liquid crystal spatial light modulator", Proc. SPIE 8161, Atmospheric Optics IV: Turbulence and Propagation, 81610H (6 September 2011); https://doi.org/10.1117/12.903681

[8] Peter Jacquemin, Bautista Fernandez, Christopher C. Wilcox et al., "Deep Horizontal Atmospheric Turbulence Modeling and Simulation with a Liquid Crystal Spatial Light Modulator", pg. , (2012).

[9] C. O. Font et al., "Implementation of a Phase only Spatial Light Modulator as an Atmospheric Turbulence Simulator at 1550 nm," Advances in Optical Technologies, Vol 2014, 167129, (2014).

[10] Italo Toselli, Olga Korotkova, Xifeng Xiao, and David G. Voelz, "SLM-based laboratory simulations of Kolmogorov and non-Kolmogorov anisotropic turbulence," Appl. Opt. 54, 4740-4744 (2015)

[11] Carolina Rickenstorff, José A. Rodrigo, and Tatiana Alieva, "Programmable simulator for beam propagation in turbulent atmosphere," Opt. Express 24, 10000-10012 (2016).

[12] Y. K. Chahine, S. A. Tedder, B. Floyd, and B. E. Vyhnalek, "Verification of the mode fidelity and Fried parameter for optical turbulence generated by a spatial light modulator," Opt. Continuum 1, 2112-2126 (2022).

[13] J. D. Phillips, M. E. Goda, and J. Schmidt, "Atmospheric turbulence simulation using liquid crystal spatial light modulators," in Advanced Wavefront Control: Methods, Devices, and Applications III, vol. 5894. M. T. Gruneisen, J. D. Gonglewski, and M. K. Giles, eds., International Society for Optics and Photonics (SPIE, 2005), pp. 57 – 67.

[14] M. Otsubo, H. Takami, and M. Iye, "Holographic atmospheric turbulence simulator for testing adaptive optics systems". Publ. Astronom. Soc. Pac. 109(739) (1997) 1057

[15] S. Thomas, "A simple turbulence simulator for adaptive optics," Proc. SPIE 5490, 766-773 (2004).

[16] S. K. Mishra, A. Dixit, V. Porwal, and D. Mohan, Design and testing of customized phase plate as atmospheric turbulence simulator. In Proc. XXXVII OSI symposium (Pond. Univ.) (2013) pp. 172-174. https://doi.org/10.13140/2.1.4106.5920.
[17] Jun Ho Lee, Sunmy Shin, Gyu Nam Park, Hyug-Gyo Rhee, and Ho-Soon Yang, "Atmospheric Turbulence Simulator for Adaptive Optics Evaluation on an Optical Test Bench," Curr. Opt. Photon. 1, 107-112 (2017).
[18] Awakash Dixit, Vikash Porwal, Ajay Kumar et al., "Systematic Characterization of Near-Index-Matched Optics Based Atmospheric Turbulence Simulator", MAPAN 35(2), pg. 221, (2020); doi:10.1007/s12647-020-00370-9.
[19] S. A. Tedder, B. Floyd, Y. K. Chahine, B. Croop, B. E. Vyhnalek, C. Betters, and S. G. Leon-Saval, "Measurements of few-mode fiber photonic lanterns in emulated atmospheric conditions for a low earth orbit space to ground optical communication receiver application," in Free-SpaceLaser Communications XXXII, vol. 11272, International Society for Optics and Photonics (SPIE, 2020), pp. 183 – 192.
[20] V. Arrizón, U. Ruiz, R. Carrada, and L. A. González, "Pixelated phase computer holograms for the accurate encoding of scalar complex fields," J. Opt. Soc. Am. A **24**, 3500–3507 (2007).
[21] Meadowlark optics. "Meadowlark Optics", https://www.meadowlark.com/, (30 November 2022).
[22] Shane, J. C., McKnight, D. J., Hill, A., Taberski, K. and Serati, S., "Designing a new spatial light modulator for holographic photostimulation," Opt. Trapp. Opt. Micromanipulation XVI 11083, K. Dholakia and G. C. Spalding, Eds., 3, SPIE (2019). https://doi.org/10.1117/12.2528558.
[23] David Benton, Andrew Ellis, Yiming Li and Zhouyi Hu, "Emulating atmospheric turbulence effects on a micro-mirror array: assessing the DMD for use with free-space-to-fibre optical connections", Engineering Research Express, Vol. 4, No. 4. (2022).
[24] M. Spivack and B. Uscinski, "The split-step solution in random wave propagation," J. Comput. Appl. Math. 27, 349 – 361 (1989).
[25] Y. K. Chahine, S. A. Tedder, B. E. Vyhnalek, and A. C. Wroblewski, "Beam propagation through atmospheric turbulence using an altitude-dependent structure profile with non-uniformly distributed phase screens," in Free-Space Laser Communications XXXII, vol.11272 H. Hemmati and D. M. Boroson, eds., International Society for Optics and Photonics (SPIE, 2020), pp. 263 – 277.
[26] B. Rodenburg, M. Mirhosseini, M. Malik, O. S. Magaña-Loaiza, M. Yanakas, L. Maher, N. K. Steinhoff, G. A. Tyler, and R. W. Boyd, "Simulating thick atmospheric turbulence in the lab with application to orbital angular momentum communication," New J. Phys. 16, 033020 (2014).
[27] M. Spencer, R. Raynor, T. Rhoadarmer, and D. Marker, "Deep turbulence simulation in a scaled-laboratory environment using five phase-only spatial light modulators," in Proc. 18th Coherent Laser Radar Conf, (2016).
[28] C. Rickenstorff, J. A. Rodrigo, and T. Alieva, "Programmable simulator for beam propagation in turbulent atmosphere," Opt. Express 24, 10000–10012 (2016).
[29] S. Cavazzani, S. Ortolani, and C. Barbieri, "Fluctuations of photon arrival times in free atmosphere," Mon. Notices Royal Astron. Soc. 419, 2349–2355 (2012).

APPENDIX A: SYSTEM TRANSFER OPERATOR FOR TURBULENCE EMULATION

The holographic system described in this work can be used to produce turbulent spatial modes emulating the light arriving at an optical receiver after propagation through the atmosphere. This receiver-side emulation capability is sufficient for many applications, including evaluating the coupling efficiency of receiver optical devices and in-hardware testing of adaptive optics systems in the presence of branch points and intensity nulls. However, this capability differs from an "operational" emulation system as it does not directly mimic the action of the atmosphere on an arbitrary input beam. More precisely, the transfer operator $u_o = H_{atm}u_i$ for an atmospheric channel, relating the optical field $u_i(x,y)$ of a monochromatic beam at an input plane to the field $u_o(x,y)$ at the output plane can be approximated as Refs. [24, 25].

$$H_{atm} = A_p(x,y)e^{-iP^2\Delta z_n}e^{i\phi_n}\dots e^{-iP^2\Delta z_1}e^{i\phi_1} \quad (1)$$

where $A_p(x,y)$ is the receiver pupil function, $\phi_i(x,y)$ is the phase perturbation accumulated through a single atmospheric layer, and $e^{-iP^2\Delta z_i}$ is the Fresnel operator for vacuum propagation through a distance Δz_i. On the other hand, using the SLM as a hologram using the method of Refs. [20, 22], the transfer operator H_{holo} for the holographic system from the input to the SLM-plane to the 4f-plane is a multiplication operator

$$H_{holo} = A(x,y)e^{i\phi(x,y)} \quad (2)$$

It is evident that the two operators coincide only when the approximation (1) is limited to a single layer $e^{i\phi_1}$.

A direct approach to emulate the full transfer operator (1) is to employ multiple SLMs as phase screens separated by small free-space sections for propagation between layers[13, 26, 27, 28]. However, in addition to the increased complexity of such a system, the use of multiple SLMs can lead to diffractive artifacts when the beam overfills the SLM aperture[13]. Such overfilling is natural when emulating systems for astronomy and space-to-ground laser communication due to the large beam footprint at the atmospheric entry plane. In such cases, the input beam may be modeled as a plane wave field and full emulation of the transfer operator for an arbitrary input beam may not be a strict requirement.

For example, in Ref.[12] the split-step beam propagation method was used to determine the action of H_{atm} on a plane wave input in order to construct the hologram. In principle, no measurement of the resulting optical field $u_o(x,y)$ made by a receiver after the 4f plane can distinguish the holographic channel H_{holo} from the atmospheric channel H_{atm} used to generate the hologram. This is possible due to the non-unitarity of the channels—information is discarded by the spatial filter in the holographic channel and by the pupil function in the atmospheric channel. Of course, for optical communication applications one might be interested in emulating pulse propagation which is not strictly monochromatic, where both geometric path delay[29] and chromatic dispersion from the diffractive SLM hologram can distinguish the channels (although the latter is generally negligible for a quasi-monochromatic beam $\Delta\lambda/\lambda \ll 1$).

To summarize, emulation via the holographic technique may be acceptable when either

(1) the atmosphere can be approximated as a thin phase screen,
(2) only receiver-side channel emulation is required, or
(3) light entering the atmospheric channel can be assumed to occupy a single plane-wave spatial mode.

The first condition is generally invoked when employing a single SLM or phase plate as a phase screen; however, holographic techniques also enable emulation of a multi-layer atmosphere using a single SLM provided either of the latter conditions are satisfied. On the other hand, for applications where the atmospheric channel acts on light in many spatial modes, such as free-space communication with orbital angular momentum (OAM) or partially coherent beams, direct emulation of the channel transfer operator H_{atm} may be required[29].